J. Plasma Physics (2002), *vol.* 68, *part* 3, *pp.* 161–172.
DOI: 10.1017/S0022377802001939 Printed in the United Kingdom

Letter to the Editor

Particle acceleration by lower-hybrid turbulence

R. BINGHAM, J. M. DAWSON† [a] and V. D. SHAPIRO[b]

Rutherford Appleton Laboratory, Chilton, Didcot, Oxfordshire OX11 0QX, UK
(r.bingham@rl.ac.uk)

(Received 11 December 2001)

Abstract. We investigate particle acceleration by strong lower-hybrid turbulence produced by the relaxation of an energetic perpendicular ion ring distribution. Ion ring distributions are associated with counterstreaming plasma flows in a magnetic field, and are found at perpendicular shocks as a result of ion reflection from the shock surface. Using a $2\frac{1}{2}$D particle-in-cell (PIC) code that is fully electromagnetic and relativistic, we show that the ion ring is unstable to the generation of strong plasma turbulence at the lower-hybrid resonant frequency. The lower-hybrid wave turbulence collapses in configuration space, producing density cavities. The collapse of the cavities is halted by particle acceleration, producing energetic electron and ion tails. For solar flare plasmas with temperatures of 1 keV and a ratio of the plasma frequency to the electron cyclotron frequency of $\frac{1}{2}$, we demonstrate electron acceleration to energies up to MeV, while the ions are accelerated to energies in the region of several MeV.

1. Introduction

Acceleration of charged particles in collisionless shocks is either directly observed or inferred from the radiation signatures. These shocks are believed to be associated with the generation of non-thermal particle populations in many space and astrophysical plasmas, including bow shocks, solar flares, stellar winds, supernova remnants and radio jets. A key dissipation mechanism in quasiperpendicular shocks is the ion reflection from the sharp potential rise that sometimes gives rise to a broad shallow foot in the magnetic profile. Clear evidence of the foot and reflected ions was found at the Earth's bow shock by Paschmann et al. (1982). These reflected ions form a counterstreaming ion flow, and can form a ring distribution

† This paper was completed just before the unfortunate death of Professor John Dawson, whom we all miss dearly. Although he is gone, his spirit lives on, and this paper is dedicated to him and his life.

[a] Department of Physics, University of California, Los Angeles, California 90024-1547, USA

[b] Department of Physics, University of California, San Diego, La Jolla, CA 92093-0319, USA email-vshapiro@ucsd.edu

in velocity space perpendicular to the magnetic field. Anisotropic ion distributions such as velocity ring distributions have been observed at the Earth's bow shock (Paschmann et al. 1982) and in computer simulations (Lembege and Dawson 1986) of perpendicular shocks. Similar ion ring configurations are found in counterstreaming plasma flows such as in the plasma mantle of non-magnetized planets (Shapiro et al. 1995b) and in cometary atmospheres (Johnstone et al. 1988) and in stellar wind interactions with plasma or neutral gas clouds. Instabilities for which the source of free energy is an anisotropic ion distribution, such as a ring distribution (Akimoto et al. 1985), or a cross-field current (i.e. the modified two-stream instability: McBride et al. 1972) are likely to produce waves around the lower-hybrid frequency for low- or moderate-β plasmas. Lower-hybrid waves are extremely important in transferring energy between different particle populations and fields in both astrophysical and laboratory plasmas because these waves can be in Landau resonance simultaneously with both the relatively slow ions and fast electrons. This is possible since the waves have both a wavenumber and an electric field parallel and perpendicular to the magnetic field such that $k_{||}/k_{\perp} \approx (m_e/m_i)^{1/2}$, where $k_{||,\perp}$ are the parallel and perpendicular wavenumbers with respect to the ambient magnetic field. When $k_{||} \ll k_{\perp} \approx k$, the resonance conditions $\omega \approx kv_i \approx k_{||}v_e$ are simultaneously satisfied for $v_e \gg v_i$, where v_e is the electron velocity and v_i is the ion velocity.

The excitation of lower-hybrid waves by the anisotropic ion ring distribution and subsequent wave–particle interactions is thus a mechanism for transferring the energy in the shock into energetic electrons and ions. This can be one of the main dissipation mechanisms in quasiperpendicular shocks. It can easily be demonstrated theoretically (Woods 1969) that a sizeable fraction of ions are indeed reflected from a perpendicular shock. Paschmann et al. (1982) have observed that about 20% of ions form the ring distribution. Numerical simulations of quasiperpendicular shocks by Quest (1986) also show the presence of reflected ions. These reflected ions therefore constitute a major shock-dissipation mechanism.

A number of modes can be excited by ring distributions (Akimoto et al. 1985) – for example, whenever the ion ring and background ion population are considered to be magnetized, ion-cyclotron waves are generated (Shafranov and Sagdeev 1961). If the ions are unmagnetized and the electrons magnetized then waves in the lower-hybrid frequency range are generated and can involve either ion–ion or electron–ion interactions. Ion-acoustic-like instabilities also exist, but these are only possible if the electron temperature is significantly greater than the ion temperature and if the electrons are unmagnetized. A great deal of literature involving the linear theory of ion ring distributions exists already and is summarized by Mikhailovskii (1974).

If the density of the ring particles is significant then the lower-hybrid waves can grow to large amplitudes, resulting in a strongly turbulent plasmas where there is the possibility of lower-hybrid wave collapse (Shapiro and Schevchenko 1984; Shapiro et al. 1993, 1995a,b) initiated by the modulational instability. Normally instabilities generate waves in the region of **k** space where dissipation is negligible; otherwise the waves would not grow. With the development of the modulational instability, a cascade to larger wavenumbers results, leading to wave collapse and absorption by Landau damping and transit-time or transitional damping. As a result of wave collapse, direct wave-energy transfer to the electrons and ions takes place. In order to test the wave collapse model for particle acceleration, a $2\frac{1}{2}$D particle-in-cell (PIC) code was used to simulate ion-ring relaxation under conditions

where the plasma β is small (<1). For low-β plasmas, the electrostatic modes are easy to excite. The code was previously used to explain acceleration in solar flares (McClements et al. 1990, 1993). Using the solar flare model we demonstrate in this paper that strong lower hybrid turbulence is responsible for producing both energetic electrons and ions.

2. Particle acceleration, simulations and theory

In this paper, we shall show that not only does electron acceleration take place, but also simultaneously ion acceleration. The model is general and can be used to explain acceleration of particles in solar flares (McClements et al. 1990, 1993) and astrophysical shocks, such as the acceleration of the injection particles in supernova remnants, which are then accelerated further by this or other mechanisms to cosmic-ray energies (Spicer et al. 1990; McClements et al. 1997). A similar model for energetic particle production in comets was proposed by Bingham et al. (1991) and Shapiro et al. (1999) to explain the observations of X-rays from comet Hyakutake (Lisse 1996), and coupling of the solar wind to non-magnetized planets (Shapiro et al. 1995b). The model is also applicable to the interaction of the interstellar medium with the heliosphere. Particle simulations were carried out using a fully electromagnetic, relativistic PIC code. There are two space dimensions and three velocity dimensions, with the possibility of the magnetic field lying in or out of the coordinate plane. The ratio of the proton mass m_i to the electron mass m_e is taken to be either 100 or 400. This choice of mass ratio is sufficiently large that significant electron and ion acceleration can occur within a computationally convenient interval of simulated time. The initial ion distribution consisted of a monoenergetic perpendicular (to $\mathbf{B}_0$) ring and a Maxwellian core, the ratio of the density of ring ions n_r to core ions n_c being $3:7$. This is close to density ratios observed at the Earth's bow shock (Paschmann et al. 1982). In the absence of in situ measurements, it is not possible to say with certainty that ring densities as high as this could occur in the solar or supernova-remnant case. However, our plasma parameters were chosen such that gyrating ions constituted only a small fraction (about 4%) of the energy potentially available in the downstream magnetic field. The electron gyrofrequency ω_{ce} was taken to be twice the electron plasma frequency ω_{pe}. Two different magnetic field configurations have been used, corresponding to (a) the magnetic field in the plane of the simulation and (b) the magnetic field predominantly out of the plane of the simulation. These two different situations will make it possible to decide whether or not strong turbulence effects such as the modulational instability followed by wave collapse are responsible for the acceleration. The situation where the magnetic field is out of the plane of the simulation should not result in collapse along the field and hence no cascading to larger $k_{\|}$ and therefore very little electron acceleration. Since the ions are accelerated perpendicular to $\mathbf{B}$, there should be ion acceleration in both cases, although it should be greater in the case where the magnetic field is out of the plane of the simulation.

Ion ring distributions have been shown by Mikhailovskii (1974) to excite waves in the lower-hybrid frequency range

$$\omega = \omega_{LH}\left(1 + \frac{1}{2}k^2R^2 + \frac{m_i}{2m_e}\frac{k_{\|}^2}{k^2} - \frac{\omega_{pe}^2}{2k^2c^2}\frac{\omega_{pe}^2}{\omega_{pe}^2 + \omega_{ce}^2}\right), \tag{1}$$

https://doi.org/10.1017/S0022377802001939 Published online by Cambridge University Press

with a growth rate

$$\gamma_0 \approx \frac{n_r}{n_c}\omega_{LH}, \tag{2}$$

where

$$\omega_{LH} = \frac{\omega_{pi}}{\left(1+\omega_{pe}^2/\omega_{ce}^2\right)^{1/2}},$$

is the lower-hybrid frequency

$$R = \left(\frac{3T_i}{\omega_{LH}^2 m_i} + \frac{2T_e}{\omega_{ce}^2 m_e}\frac{\omega_{pe}^2}{\omega_{pe}^2+\omega_{ce}^2}\right)^{1/2},$$

ω_{pi} is the ion plasma frequency and $T_{e,i}$ are the electron and ion temperatures. The last term in (1) is the electromagnetic correction to the frequency. Resonant oscillations grow for $\omega = \mathbf{k}\cdot\mathbf{v}_r$, where $\mathbf{v}_r$ is the velocity of the ion ring.

The initial ion distribution is given by

$$f_i(v_{||}, v_\perp) = \frac{n_c}{(2\pi)^{3/2}v_c}\exp\left(-\frac{v_{||}^2+v_\perp^2}{2v_c^2}\right) + \frac{n_r}{4\pi^2 v_r v_c^2}\exp\left[-\frac{v_{||}^2+(v_\perp^2-v_r)^2}{2v_c^2}\right], \tag{3}$$

where v_c is the core ion thermal speed and v_r is the ring speed. As stated, $n_r/n_c \approx 3/7$ and $v_r \approx 20v_c$, with $m_e/m_i = 100$ this means $v_r = 2v_e$ and with $m_e/m_i = 400$, $v_r = v_e$, where v_e is the electron thermal speed. The ion ring speeds are easily computed from knowledge of the shock Mach number. The core ion temperature, which is assumed to be equal to the initial electron temperature, was set equal to 800 eV, and for $\omega_{pe} = \frac{1}{2}\omega_{ce}$ this means that the plasma $\beta \ll 1$, ensuring that the modes excited are electrostatic in nature.

As discussed earlier, two different magnetic field configurations were used in the simulations, corresponding to (a) the magnetic field in the plane (x, y) of the simulation, $(B_{0x}, B_{0y}, 0), B_{0x} \gg B_{0y}$, and (b) the magnetic field predominantly out of the plane of the simulation, $(B_{0x}, 0, B_{0z}), B_{0z} \gg B_{0x}$. The plane of the simulation is the (x, y) plane. We should expect that for case (a) both electrons and ions would be accelerated, while for case (b) mostly the ions would be accelerated, and this is borne out in the simulations, where there is only weak electron acceleration, which we now describe.

The results of the simulation are shown in Figs 1–7. Figure 1 depicts the time evolution of the wave spectral density as a function of the parallel phase velocity; the lower-hybrid waves appear at the low phase velocity (<the speed of light c) and are seen to grow and then fall to a saturated level determined by particle absorption.

Figure 2 represents the time snaps of the electric field power spectrum for times $\omega_{pe}t$ = 0–35 (a), 400 (b), 800 (c) and 1200 (d). Note that intense low-frequency spikes appear first with a frequency around the lower-hybrid frequency. these waves are the fastest growing waves driven by the ion ring distribution. The waves have dropped to smaller values in Figs 2(b) and (c). This is a result of the waves saturating, and being absorbed by both electrons and ions. Once the waves have been depleted they no longer accelerate particles and with the ring distribution still present they can be further driven to high values as shown in Fig. 2(d). The waves are now sufficiently strong to accelerate the particles. This behaviour appears as a pulsation locally in the accelerated particles with the waves growing, saturating and

https://doi.org/10.1017/S0022377802001939 Published online by Cambridge University Press

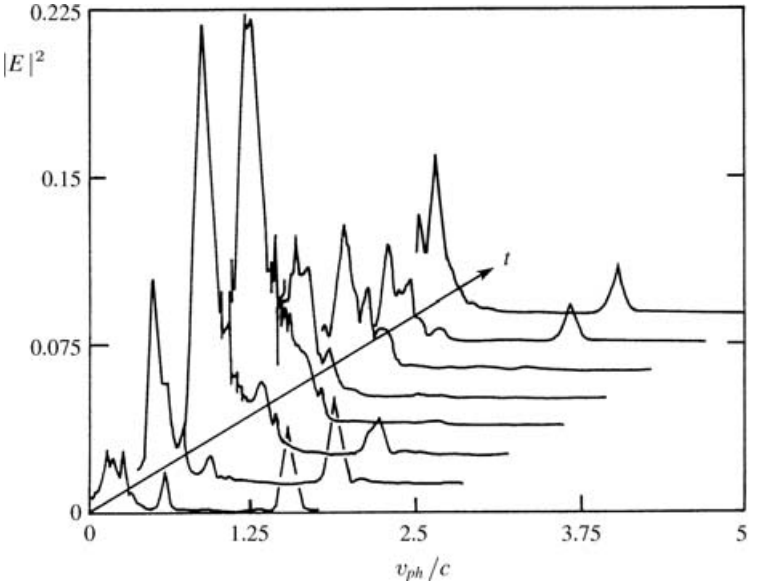

Figure 1. Time evolution of the wave spectral density as a function of the parallel phase velocity.

being absorbed. In the higher-frequency regime, emission occurs predominantly at the electron cyclotron frequency at early times (Fig. 2b).

Figure 3 represents the time evolution of wave energy density, electron energy and ring ion energy up to $\omega_{pe}t = 1500$. It should be noted that only a small fraction of the free ring ion energy ends up in the waves and most goes into electrons and ions.

Figure 4(a) represents the time evolution of the electron distribution as a function of $v_{||}$, Fig. 4(b) represents an intermediate state demonstrating the evolution of a beam, i.e. with a positive slope in $f(v_{||})$ there was very little acceleration for the case where the major component of the magnetic field was out of the plane of the simulations.

Figure 5 depicts the initial and final ion core distribution function, showing significant energization in the perpendicular plane for both types of simulation. Protons with energies in the range of 2 MeV are observed to be produced within distances of the order of 10s of metres and within a few ion-gyroperiods, both electrons and ions are observed to be accelerated in localized regions of space, indicating the presence of cavitons (Figs 6 and 7). The acceleration of electrons and ions takes place simultaneously, indicating that it is not a two-stage process but is caused by a similar mechanism in this case owing to the waves generated at the lower-hybrid resonance frequency that resonate with ions moving perpendicular to the magnetic field and with electrons moving parallel to the magnetic field. Detailed studies of the electron distribution function reveal the presence of beams with positive slopes in f_e, i.e. $\partial f_e/\partial v > 0$ (Fig. 4b). This cannot be caused by a simple quasilinear diffusion process which at best can only produce a plateau in f_e. We also find evidence for the 'fan' instability (Shapiro and Shevchenko 1968, Kadomtsev and Pogutse 1967) which results in pitch angle scattering of the electrons and

https://doi.org/10.1017/S0022377802001939 Published online by Cambridge University Press

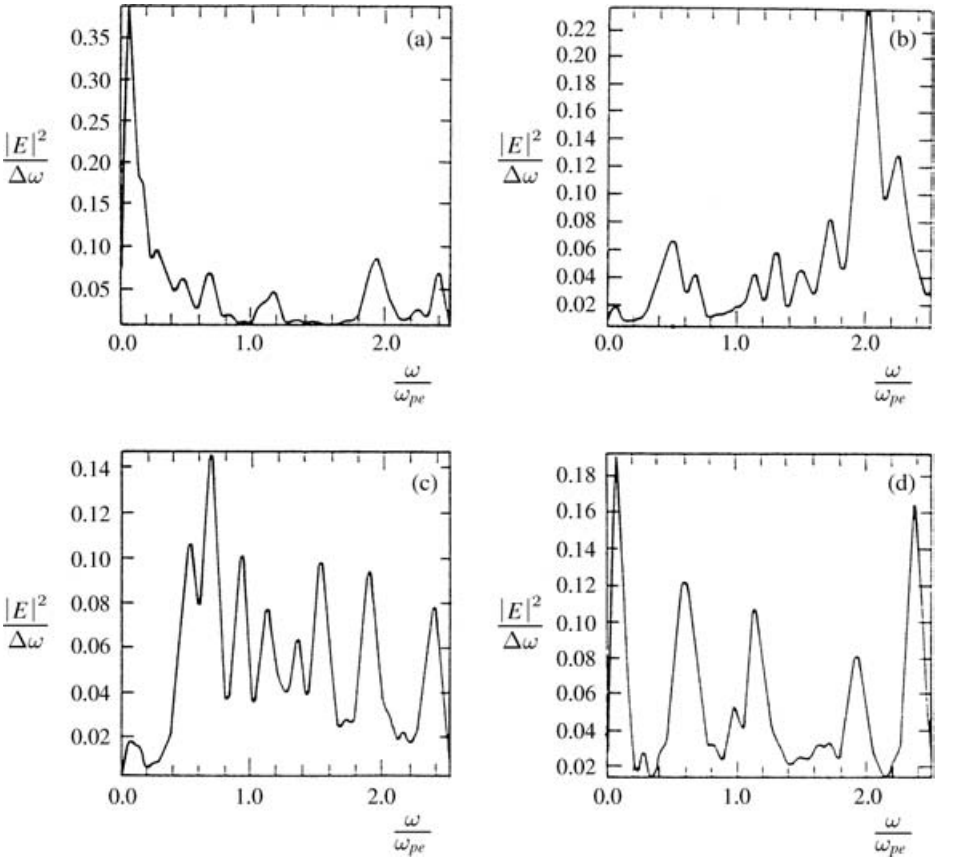

Figure 2. Electric field power spectrum at $\omega_{pe}t = 0$–350 (a), 400 (b), 800 (c) and 1200 (d). The intense low-frequency spikes in (a) and (d) occur around the lower-hybrid resonance frequency. In the microwave range, emission occurs predominantly at the electron cyclotron frequency at early times and at the upper hybrid frequency at later times.

generation of synchrotron radiation. The most energetic part of the electron distribution function corresponds to the field aligned electron tail descending with energy. This part of the distribution can be easily obtained from the quasilinear diffusion equation, the tail can also drive the excitation of electron whistler waves. The mechanism of the 'fan' instability is based on anomalous Doppler resonance of electrons with waves such that $\omega - k_{||}v_{||} = -\omega_{ce}$, the source of instability is the anisotropic electron velocity distribution and not in the positive slope. Waves with frequencies $\omega < \omega_{ce}$ are excited and pitch angle scattering by the waves creates a positive slope on the electron distribution function. We find that at the end of the simulations approximately 10% of the ring energy has been transferred to the background electrons and ions, while less than 1% of the energy is stored in all the waves generated. Test particle trajectories and the time history of the parallel momenta for test particles are shown in Figs 6(a) and (b). These test particles are electrons that are accelerated parallel to the magnetic field along thin filaments, which would not be expected from a uniform isotropic distribution of turbulence. Figure 6(a) depicts the plane of acceleration, while Fig. 6(b) is orthogonal

https://doi.org/10.1017/S0022377802001939 Published online by Cambridge University Press

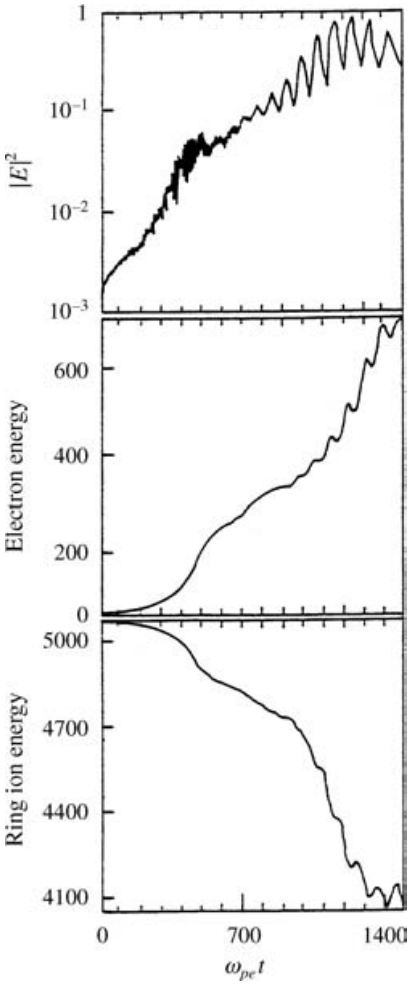

Figure 3. Time evolution of wave energy density electron kinetic energy and ion ring kinetic energy.

to this plane, showing the cross section of the filaments. The filamentary nature indicates that acceleration is taking place in narrow structures similar to what one would expect from wavepackets confined to relatively thin structures aligned along the magnetic field. These structures would be consistent with the collapse of lower-hybrid waves, which form cigar-shaped nonlinear wavepackets aligned along the magnetic field. These nonlinear wavepackets form caviton-like structures, which are regions of intense wave activity in density depressions or density holes (Fig. 7). These density holes are also a signature of strong turbulence. We find that no filamentary structures or significant electron acceleration occurs when the magnetic field is out of the plane of the simulation. An analysis of the spatial structure of the density perturbations, electric field envelope and magnetic field structure reveals the presence of wave collapse – it is within the collapsing nonlinear wavepackets that strong acceleration is found. The caviton size is proportional to

https://doi.org/10.1017/S0022377802001939 Published online by Cambridge University Press

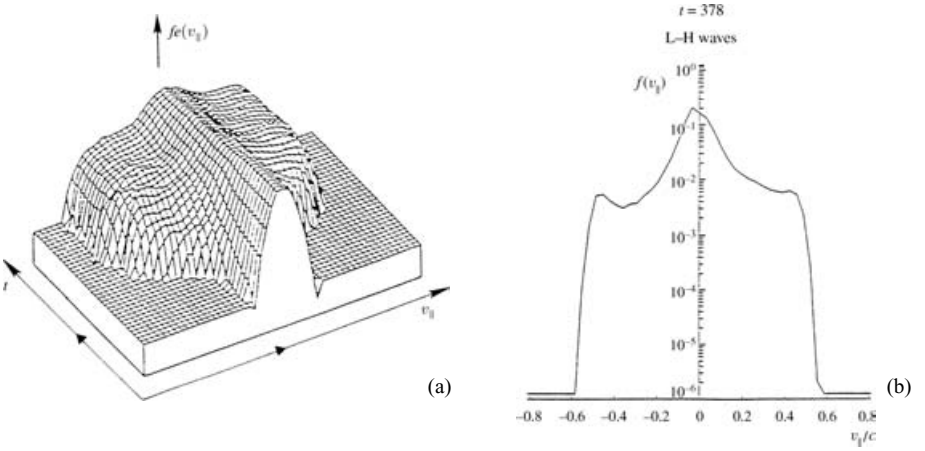

Figure 4. (a) Parallel component of the electron distribution function as a function of time and (b) showing a bump on the tail.

the ion-to-electron mass ratio; for example, the transverse width $L_\perp \approx 1.5c/\omega_{pe}$ for $m_i/m_e = 100$ and $L_\perp \approx 6c/\omega_{pe}$ for $m_i/m_e = 400$ with $L_{||}/L_\perp \approx (m_i/m_e)^{1/2}$, where $L_{||}$ is the longitudinal length. An analysis of the spectral components reveals the presence of large $k_{||}$, indicating that the modulational instability has occurred which is responsible for this observation. The large-$k_{||}$ wave components have small phase velocities and can therefore interact with the main part of the electron distribution function producing a high energy tail. One of the most interesting aspects of the simulation is the appearance of the low-frequency magnetic field perturbation associated with the density structures. The appearance of a magnetic perturbation is a result of the low-frequency mode that is driven by the high-frequency lower-hybrid waves (i.e. the magnetosonic model). Normally the low-frequency mode is associated with the ion acoustic wave, which in our case is replaced by the magnetosonic wave. An analysis of the modulational instability of lower-hybrid waves in which the slowly varying low-frequency mode is associated with the magnetosonic mode with the instability resulting in magnetic field modulations, Fig. 4(b), has been carried out by Bingham et al. (1991). The equations describing the modulational instability can be written in the form

$$\frac{2}{i\omega_{LH}}\frac{\partial}{\partial t}\nabla_\perp^2\phi - R^2\nabla_\perp^4\phi + \frac{m_i}{m_e}\frac{\partial^2\phi}{\partial z^2} = \mathscr{A}\nabla_\perp\cdot\left[\left(\frac{\delta n}{n_0}-\frac{\delta B}{B_0}\right)\nabla_\perp\phi\right] + \mathscr{B}\frac{\partial}{\partial z}\left[\left(\frac{\delta n}{n_0}-\frac{\delta B}{B_0}\right)\frac{\partial\phi}{\partial z}\right] - \frac{m_i}{m_e}\frac{\omega_{LH}}{i\omega_{ce}}\left[\nabla\phi\times\nabla\left(\frac{\delta n}{n_0}-\frac{\delta B}{B_0}\right)\right]_z \quad (4)$$

$$\frac{\partial^2}{\partial t^2}\delta n - \frac{T}{m_i}\nabla_\perp^2\delta n = -\frac{1}{16\pi m_i}\nabla_\perp^2\left[\mathscr{A}|\nabla_\perp\phi|^2 + \mathscr{B}\left|\frac{\partial\phi}{\partial z}\right|^2 + \mathscr{C}(\nabla\phi^*\times\nabla\phi)_z\right], \quad (5)$$

where

$$\mathscr{A} = \frac{\omega_{pi}^2}{\omega_{LH}^2} - \frac{\omega_{pe}^2}{\omega_{ce}^2}, \quad \mathscr{B} = \frac{\omega_{pe}^2}{\omega_{LH}^2} + \frac{\omega_{pi}^2}{\omega_{LH}^2} \approx \frac{\omega_{pe}^2}{\omega_{LH}^2}, \quad \mathscr{C} = \frac{i\omega_{pe}^2}{\omega_{LH}\omega_{ce}}.$$

and z is used to indicate direction $\parallel$ to B.

https://doi.org/10.1017/S0022377802001939 Published online by Cambridge University Press

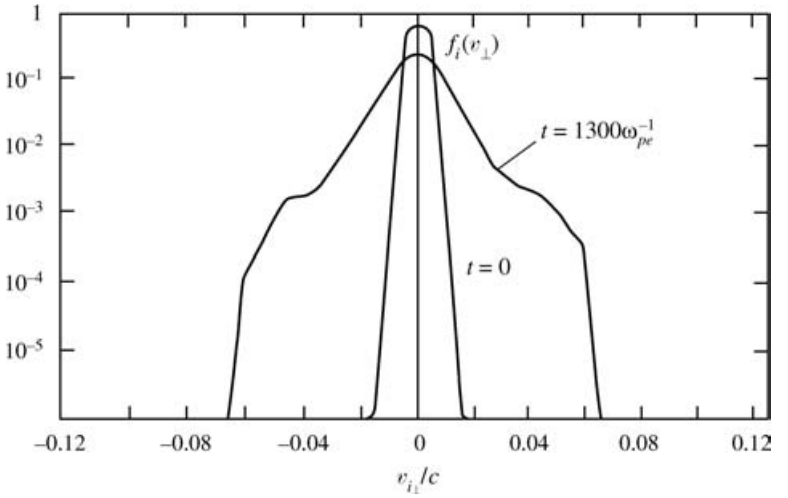

Figure 5. Core ion distribution function in perpendicular velocity space at $\omega_{pe}t = 0$ and 1300. The ion acceleration is up to several MeV and is predominantly in the perpendicular direction.

The density δn and magnetic field δB perturbations are related by the usual relation namely $\frac{\partial^2}{\partial t^2}\frac{\delta n}{n_0} = v_A^2 \nabla_\perp \frac{\delta B}{B_0}$, where v_A is the Alfv́en velocity. This relation is a consequence of quasineutrality of the slow magneto-acoustic wave, i.e. $\delta n_e = \delta n_i$. The notation $\nabla_\perp^2$ represents the two-dimensional (2D) Laplacian operator in the plane perpendicular to the magnetic field, where $\phi(t, \mathbf{r})$ is the complex amplitude of the lower-hybrid electrostatic potential.

In equation (5) $|\nabla_\perp \phi|^2$ and $|\partial\phi/\partial z|^2$ terms are obtained from the normal ponderomotive force expression acting perpendicular and parallel to the magnetic field B_0. The nonlinear force is produced by the Reynolds stress in the electron field aligned motion, namely $(v_e \cdot \nabla) v_{e||}$.

In a three-dimensional (3D) treatment of the problem these terms are negligible in comparison with the vector nonlinearity $(\nabla\phi^* \times \nabla\phi)_z$. However, in the $2\frac{1}{2}$D simulations where the vector nonlinearity vanishes and the normal ponderomotive force terms become important and produce the collapse seen in the simulations. In this case there is no cascade to larger wavenumbers along the magnetic field which means that the lower-hybrid wave wavenumber along $\mathbf{B}_0$ is always small and therefore have velocities along $\mathbf{B}_0$ much larger than v_{Te} and only weak acceleration of electrons takes place. Only wavenumbers perpendicular to $\mathbf{B}_0$ cascade and only ion acceleration can take place for this case. This is not the case when $\mathbf{B}_0$ is in the plane of the simulation, then not only can we have perpendicular cascading in wavenumber but also cascading in the parallel direction resulting in strong acceleration of both electrons and ions. This is the reason why we only observe strong electron acceleration in the simulations when $\mathbf{B}_0$ is in the plane of the simulation grid. However, we always observe ion acceleration. In a fully 3D simulation we would always have both particles accelerated.

For a sufficiently strong pump when the threshold condition

$$\frac{k_{0y}}{k_y}\frac{c^2|E_0|^2}{B_0^2} > \frac{\omega_{LH}^2}{k^2}\frac{m_i}{m_e}\frac{k_{||}^2}{k^2} \tag{6}$$

https://doi.org/10.1017/S0022377802001939 Published online by Cambridge University Press

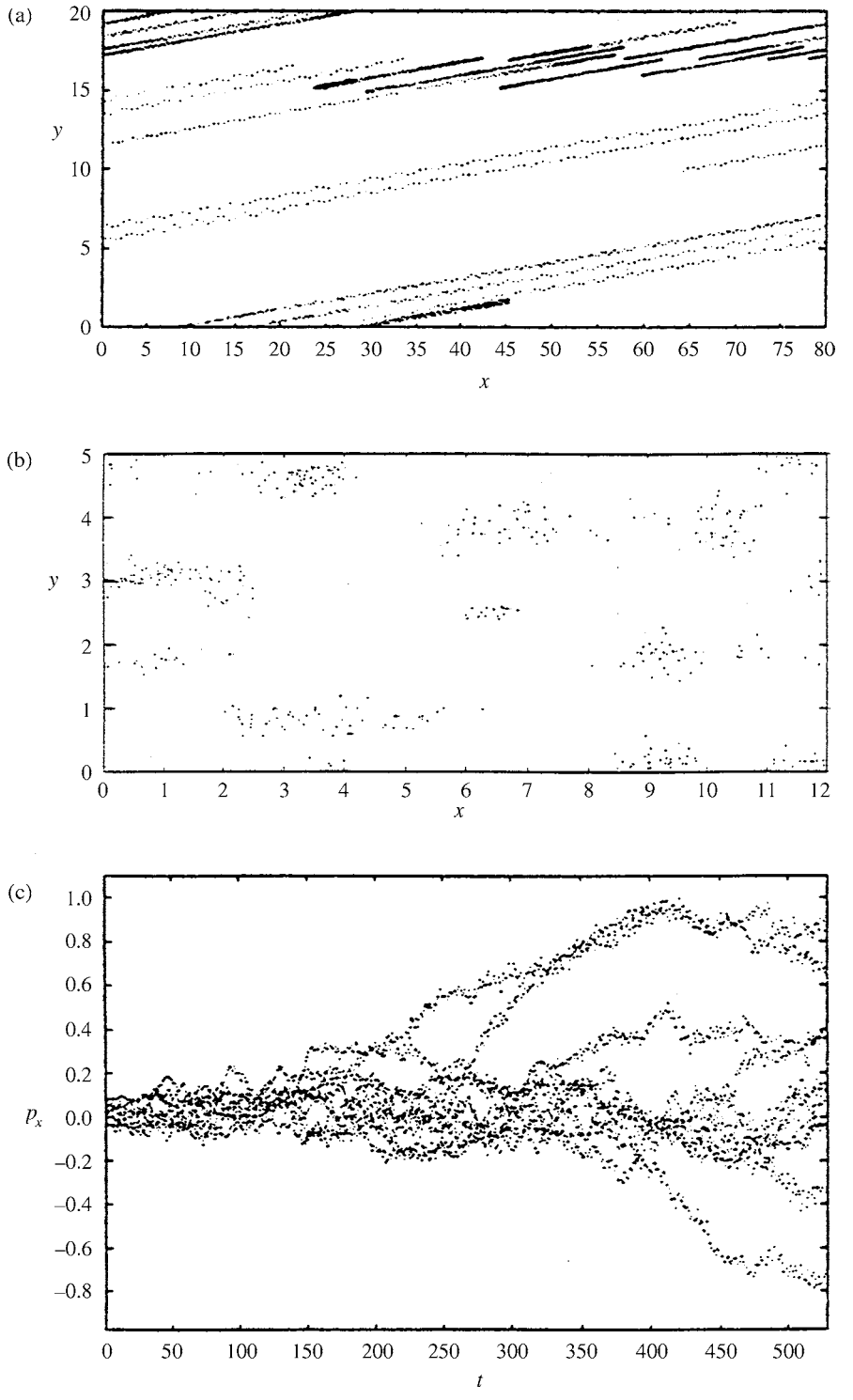

Figure 6. (a) Test particle trajectories of electrons showing acceleration along $\mathbf{B}_0$. (b) Energetic test particle electron positions in the plane perpendicular to acceleration. (c) Time history of test particle parallel momentum.

https://doi.org/10.1017/S0022377802001939 Published online by Cambridge University Press

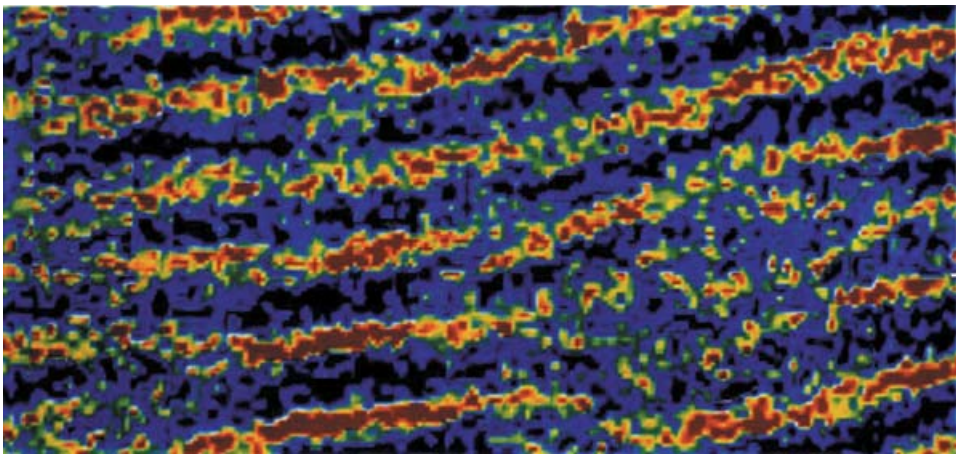

Figure 7. Caviton structures in the magnetic field direction, red indicates a more pronounced caviton density depression and stronger field strength.

is fulfilled the maximum growth rate is equal to

$$\gamma_{max} = \frac{\sqrt{3}}{2^{2/3}} \left[\omega_{LH} \frac{k_{0y}}{k_y} (\mathbf{k}_0 \times \mathbf{k})_z^2 \frac{c^2 |\phi_0|^2}{B_0^2} \right]^{1/3} . \tag{7}$$

This is for the situation where the vector nonlinearity is important. For the scalar nonlinearity the growth rate is much smaller by the factor $(m_e/m_i)^{1/2}$ and the threshold is correspondingly higher. In the $2\frac{1}{2}$D simulations carried out only the scalar nonlinearity plays a role and only in a fully 3D simulation can the vector nonlinearity by dominant. In our $2\frac{1}{2}$D simulation the strength of the coupling is weaker and the growth rate less by a factor of $(m_e/m_i)^{1/2}$.

The modulational instability not only results in the creation of magnetic structures slowly varying with time but also in the appearance of lower-hybrid wave spectrum waves with $k_{||} \neq 0$. The waves with $k_{||} \sim \frac{1}{3v_{Te}} \omega_{LH}$ will be efficiently absorbed by resonant electrons, this absorption will prevent growth of the pump amplitude causing saturation of the pump wave. In the stationary situation the rate of flow of energy into the ion-ring-driven lower-hybrid transverse mode, i.e. $\gamma_0 |E_0|^2$ must be balanced by the rate of energy flow into the oblique mode by the modulational instability, i.e. $\gamma_{max} (m_e/m_i)^{1/2} |E|^2$. The fact that the growth rate of the ring ion instability γ_0 is of the order of that for the modulational instability $\gamma_{max} (m_e/m_i)^{1/2}$ results in comparable amplitudes of transverse and oblique modes.

We have investigated electron and ion acceleration, via $2\frac{1}{2}$D PIC simulations. The free energy is provided by ions which have a ring distribution perpendicular to the magnetic fields. Ion ring distributions may be produced by either magnetic tubes merging from the photosphere or by shocks associated with coronal mass ejection (CME) or in supernova remnants. They are also associated with counterstreaming plasma flows in a magnetic field, which occur in solar wind cometary atmosphere interactions, plasma mantles of non-magnetic planets and the interstellar medium (ISM) interacting with the heliosphere. Such ring distributions are unstable to the generation of lower-hybrid waves. These lower-hybrid waves are concentrated into localized cavity structures via the modulational instability and can accelerate electrons along the field direction $\mathbf{B}_0$ and ions perpendicular to $\mathbf{B}_0$.

https://doi.org/10.1017/S0022377802001939 Published online by Cambridge University Press

Simulations show the transfer of perpendicular ion energy to energetic electrons via the process described above. The results have shown that perpendicular shocks, such as might be associated with solar flares, coronal mass ejection or supernova remnant shocks, produce ion ring distributions. Protons are accelerated to energies of tens of MeV in the same time scale. This mechanism for particle acceleration could account for the injection population of cosmic ray particles in supernova remnants.

Acknowledgements

The authors would like to acknowledge the work of J. J. Su, who undertook the early simulations described in this article.

References

Akimoto, K., Papadopoulos, K. and Winske, D. B. 1985 *J. Plasma Phys.* **34**, 445.

Bingham, R., Shapiro, V. D., Tsytovich, V. N., de Angelis, U., Gilman, M. and Shevchenko, V. I. 1991 *Phys. Fluids* **3**, 1728.

Johnstone, A. et al. 1988 *Exploration of Halley's Comet* (ed. M. Grewing, F. Praderie and R. Reinhard). Berlin: Springer-Verlag, p. 25.

Kadomtsev, B. B. and Pogutse, O. P. 1967 *Sov. Phys. JETP* **26**, 1146.

Lembege, B. and Dawson, J. M. 1986 *Phys. Fluids* **29**, 821.

Lisse, C. M., Dennerl, K., Englhauser, J., Harden, M., Marshall, F. E., Mumma, M. J., Petre, R., Pye, J. P., Ricketts, M. J., Schmidt, J., Trumfer, J. and Wert, R. G. 1996 *Science* **274**, 205.

McBride, J. B., Ott, E., Jay, P. B. and Orens, J. H. 1972 *Phys. Fluids* **157**, 2367.

McClements, K. G., Su, J. J., Bingham, R., Dawson, J. M. and Spicer, D. S. 1990 *Solar Phys.* **130**, 229.

McClements, K. G., Bingham, R., Su, J. J., Dawson, J. M. and Spicer, D. S., 1993 *Astrophys. J.* **409**, 465.

McClements, K. G., Dendy, R. O., Bingham, R., Kirk, J. G. and O'C Drury, L. 1997 *Mon. Not. R. Astron. Soc* **291**, 241.

Mikhailovskii, A. B. 1974 *Theory of Plasma Instabilities*, Vol. 1. New York: Consultants Bureau.

Paschmann, G., Sckopke, N., Bame, S. J. and Gosling, J. T. 1982 *Geophys. Res. Lett.* **9**, 881.

Quest, K. B. 1986 *J. Geophys. Res.* **91**, 8805.

Shafranov, V. D. and Sagdeev, R. Z. 1961 *Sov. Phys. JETP* **12**, 130.

Shapiro, V. D. and Shevchenko, V. I. 1968 *Sov. Phys. JETP* **27**, 635.

Shapiro, V. D. and Shevchenko, V. I. 1984 In: *Basic Plasma Physics: Handbook of Plasma Physics*, Vol. II (ed. A. A. Galeev and R. N. Sudan). Amsterdam: North-Holland, p. 123.

Shapiro, V. D., Shevchenko, V. I., Solovev, G. I., Kalinin, V. P., Bingham, R., Sagdeev, R. Z., M Ashour-Abdalla, Dawson, J. M. and Su, J. J. 1993 *Phys. Fluids* **B5**, 3148.

Shapiro, V. D., Solovev, G. I., Dawson, J. M. and Bingham, R. 1995a *Phys. Plasma* **2**, 516.

Shapiro, V. D., Szego, K., Ride, S. K., Nagy, A. F. and Shevchenko, V. I. 1995b *J. Geophys. Res.* **100**, 21 289.

Shapiro, V. D., Bingham, R., Dawson, J. M., Dobe, Z., Kellett, B. J. and Mendis, D. A. 1999 *J. Geophys. Res.* **104**, 2537.

Spicer, D. S., Clark, R. W. and Maran, S. P. 1990 *Astrophys. J.* **356**, 549.

Woods, L. C. 1969 *J. Plasma Phys.* **3**, 435.